SAND2013-1628C

On/Off Micro-electromechanical Switching of AlN Piezoelectric Resonators

Christopher D. Nordquist[1], Roy H. Olsson III[1], Sean. M. Scott[2], Darren. W. Branch[1], Tammy Pluym[1], and Victor Yarberry[1]

[1]Sandia National Laboratories, Albuquerque, NM, 87185, USA

[2]Purdue University, West Lafayette, IN, 47907, USA

Abstract — We report the first switchable piezoelectric resonator as a building block for a new class of adaptive and reconfigurable filters. The resonator integrates AlN contour-mode resonator and RF MEMS capacitive switch technologies to change the coupling between the RF signal electrodes and the AlN piezoelectric film. Modeling reveals that a 1.5 µm gap minimizes coupling, while a 10 nm gap couples nearly as efficiently as an electrode in intimate contact, suggesting that high contrast can be achieved using this approach. Measurements of a 400 µm x 150 µm two-port resonator demonstrate a switching ratio of 13 dB, a Q of 170, and a center frequency of 240 MHz. Research is continuing with goals of improving the device Q and switching ratio, extending the device operation to other frequencies, and extending the approach to adaptive and reconfigurable filters.

Index Terms — Piezoelectric transducers, resonator filters, radiofrequency microelectromechanical systems, acoustic devices.

I. Introduction

High-Q reconfigurable and adaptive filters are necessary to achieve envisioned future adaptable and reconfigurable RF systems [1]. Targeting this need, micro-electromechanical system (MEMS) reconfigurable and tunable electromagnetic filters have been demonstrated with excellent tuning range and Q's of several hundred [2,3]. However, many applications and functions with narrower bandwidths and higher selectivity require resonators with Q over 1000, which at frequencies <1 GHz are only achieved in small format with micro-electromechanical resonators [4], acoustic devices such as surface or bulk acoustic wave filters [5], or contour-mode resonators [6]. However, because acoustic resonances are determined by physical dimensions, these types of devices have limited tuning ranges and require switched filter banks to achieve appreciable frequency adaptability [7]. In this work, as a step towards reconfigurable acoustic resonators and filters, we present a method for using micro-electromechanical switching to achieve switchable acoustic resonators.

The proposed switched resonator is based on co-integration of MEMS capacitive switches with micromachined AlN contour-mode resonators. MEMS capacitive switches [8,9] and contour-mode AlN resonators [6] have been topics of research over the past decade, but to our knowledge, there have been no reports of integrating these two technologies to realize switching of piezoelectric resonances. Other relevant prior work includes capacitive switches using AlN dielectrics [10], MEMS resonators in which a suspended metal electrode allows for improved Q [11], a proposed switched BAW filter [12], and co-integration of metal contact switches with micromachined resonators [13]. However, none of these techniques demonstrate the ability to switch the piezoelectric resonance either on and off or in frequency.

In this paper, we will discuss the principle of operation for the switched resonator, the design of a specific switched two-port resonator, and present experimental evidence of a switched piezoelectric resonance.

II. Principle Of Operation

A. MEMS Resonator Switching

The principle of operation for the switched resonator is shown in Fig. 1. The upper resonator electrodes are realized using capacitive switches over the AlN piezoelectric film, and the lower electrode is a solid grounded contact. The upper electrode may be used as a transducer that is either driven by or receiving an RF signal, or may be grounded for use in a Bragg acoustic reflector. Similar to a standard capacitive switch, a DC bias voltage is applied to pull the bridges into contact with the dielectric, which in this case is an AlN piezoelectric film. In the absence of bias, the upper electrodes are separated from the piezoelectric film by a gap, resulting in low RF electric field and coupling. When a bias voltage sufficient to close the gap between the bridge and the AlN is applied, the suspended bridge collapses into intimate contact with the AlN film, coupling the RF field into the piezoelectric film.

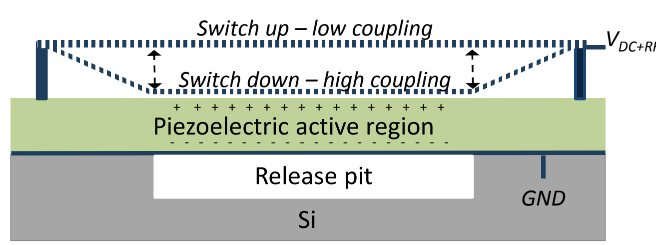

Fig. 1. Cross-section sketch of the piezoelectric switching device. When the upper electrode is separated from the piezoelectric region with a gap, coupling is weak and the resonator is off. When a bias voltage is applied, the electrode is pulled into contact by electrostatic attraction, the field in the AlN is increased, and the resonator is on.

B. Acoustic Coupling Modeling

The resonators rely on d_{31} transduction, in which the electric field is between the bridge finger and the underlying ground plane. Success of the switched resonator depends on the effectiveness of the coupling of the switch bridge to the AlN surface. To evaluate the effects of a small gap between the bridge and the AlN in the down-state, as well as the expected coupling in the up-state, finite element modeling (FEM) was used to predict the coupling-of-modes parameters (COM) parameters for a bridge with a gap of 10 nm (down) and 2 µm (up). These results were normalized to an ideal (gap = 0) contact on the 0.75 µm-thick AlN material and are summarized in Table I. For a 10 nm gap, the acoustic coupling (i.e. transduction) parameter decreases by 9% relative to the perfectly coupled case, while for the 2 µm gap the acoustic coupling is <0.1% of the ideal case, effectively turning the device off. The electrode reflection decreased rapidly for the 10 nm and 2 µm gap cases, demonstrating that the reflectivity is dominated by the mechanical contribution rather than the electrical. The low reflection for this transducer minimizes the overall phase shift across the structure. This reduces the dependence of the peak resonance on the COM reflection parameter and eases design constraints when using this approach.

TABLE I: TRANSDUCER COM PARAMETERS ($\lambda = 40$ µM)

Gap	Velocity	Reflection	Acoustic Coupling	Static Capacitance
0	1	1	1	1
10 nm	1.03	0.29	0.91	0.89
2 µm	1.03	0.03	0.03	0.05

C. Switched Resonator Design

While the described approach can be used to realize switched or reconfigurable resonators, the device described here is an on/off switched resonator. Fig. 2 shows cross-section drawings, including the strain profile, of the resonator design in both the on-state and off-state. The two half-wavelength transducer fingers are spaced on a pitch of one wavelength, with etched facets providing the reflection at the strain nulls. The total distance between the reflectors is 2.5 wavelengths. To turn the resonator off, both fingers are elevated above the substrate, reducing the electric-field coupling into the piezoelectric film.

Because the device is designed to demonstrate the switchable resonator concept in the simplest device possible, one finger was used for each of the transducers. The limited number of fingers results in a relatively high motional impedance of >1 kΩ, but allows the demonstration of the effect with only two switches. Lower motional impedance, more complex filter designs, and additional adaptability can be achieved by adding additional, individually addressed, fingers as transducers, reflectors, and coupling elements.

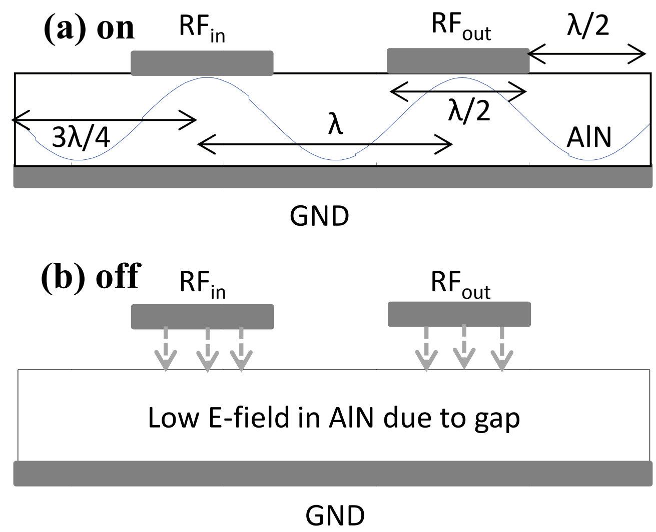

Fig. 2. Cross-section drawing of the resonator structure in the (a) on- and (b) off- state. As the fingers are separated from the substrate, the electric field and coupling reduces and the resonator turns off.

III. DEVICE FABRICATION

The cross-section of the device is shown in Fig. 3. The fabrication process consists of 10 mask layers on high-resistivity (>10 kΩ-cm) 150-mm silicon substrates and is compatible with Si CMOS electronics. The first 6 masking layers are used to fabricate the AlN resonators using processes similar to those reported previously [14]. After the resonators are fabricated, a 1.5 µm-thick Si_3N_4 dielectric film is deposited by PEVCD and chemical-mechanically polished flat to form the switch sacrificial layer, and openings are etched in this layer to make contact to the resonator metallization and anchor the switches. The switch bridge is fabricated by sputter deposition and etching of a 0.2 µm-thick Al film, followed by sputtering and etching of 1 µm-thick Al to reinforce the anchors and provide stiffness in specific beam areas. After the switch layers are completed, the Si_3N_4 switch sacrificial layer and Si resonator sacrificial layer are removed using a selective dry etch followed by XeF_2 etching.

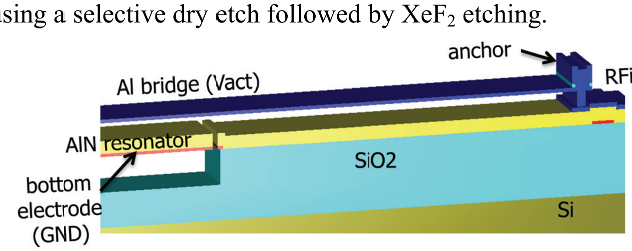

Fig. 3. Cross-section model of one-half of the bridge and resonator structure.

Fig. 4 shows optical micrographs of a switched resonator (a), a fixed down resonator (b), and a conventional resonator (c). The switched resonator fingers are comprised of fixed-fixed MEMS switches suspended over the active AlN region, the fixed-down fingers have the MEMS fingers permanently in contact with the active region, and the conventional resonators have transducer fingers that are fabricated directly on the active region. In the switched and fixed-down resonator, the RF signal is fed along the lengths of the switch bridges, while in the conventional resonator the signals are routed along the surface of the anchors. The bottom electrode is continuous underneath the AlN layer and is grounded by a trace running along the underside of the anchors. Measurements of these three variations should reveal the effects of the switch/AlN interface and the bridge feed structure. In each case described here, the resonator fingers are 20 μm wide and on a 40 μm pitch, for a resonant frequency of roughly 240 MHz. For the tested devices, the total length of the switch between the anchors is 350 μm and the distance over which the switch beam overlaps the active region is 90 μm.

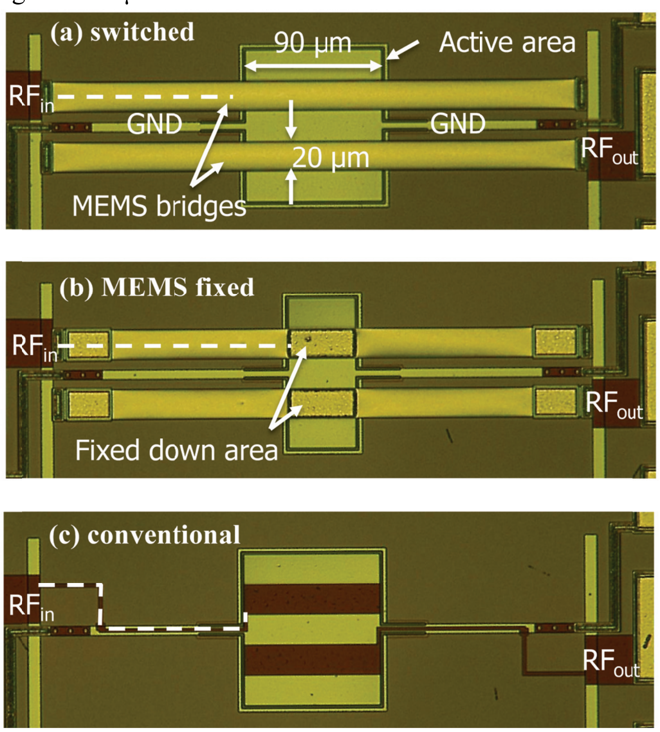

Fig. 4. Plane-view optical micrographs of (a) a switchable resonator in the off-state, (b) a "fixed-down" resonator with MEMS fingers permanently fixed to the active AlN region, and (c) a conventional resonator. The dashed lines show the routing of the RF signal from the input to the active resonator for each device type.

IV. Experimental Results

S-parameters of the switched resonator were measured at ambient temperature using GSG100 probes on a probe station with an Agilent PNA. The measurement was calibrated at the probe tips using the LRRM method, and bias was supplied to the probe tips using an external DC power supply through the internal network analyzer bias tees. The switches closed at a bias voltage of approximately 35 V between the bridge and bottom electrode. On-state measurements were taken at 40 V to ensure good switching and contact.

The insertion loss of the switched resonator is shown in Fig. 5 for the device in the on- and off- states. In the off-state, the response is dominated by approximately 20 fF of feedthrough capacitance from the bias lines and edge-coupling of the bridge. Simulations suggest that the intrinsic off-state capacitance of the bridge is 10 fF and that the isolation of the intrinsic device is at least 10 dB greater than measured. Future work will investigate reducing this feedthrough capacitance by re-routing the bias lines and redesigning the bridges for reduced edge coupling. In the on-state, the switches couple to the piezoelectric film to generate an inverting resonant response, with a peak that is 13 dB above the capacitive feedthrough. The resonator has high insertion loss because the AlN resonator material is lightly coupled through the single transducer finger. Using multiple fingers in parallel will raise the coupling, lower the motional impedance, and improve the insertion loss of the device.

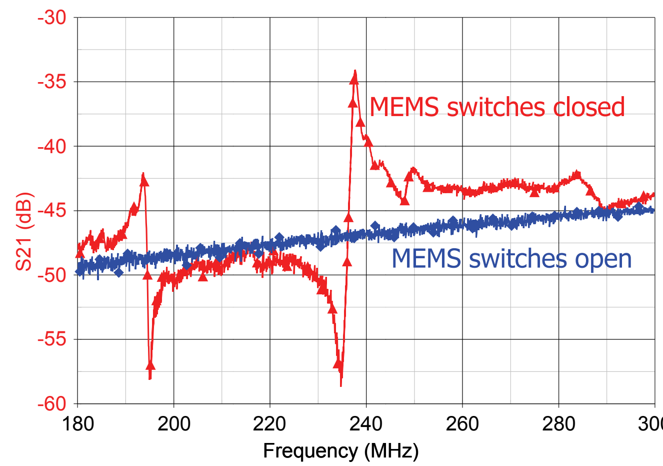

Fig. 5. Insertion loss of the switchable resonator in the off- and on-states. The off-state isolation is limited by parasitic capacitance of the bias lines and padframe.

Fig. 6 compares the response of the switched resonator to that of the same structure with the MEMS bridges fabricated in the fixed down state and to a conventional resonator with the input and output connections on the anchors of the AlN material. The response of the MEMS fixed and switched resonators are nearly identical, while the conventional design shows lower loss and higher isolation. The switched and MEMS fixed resonator Q is ~170, while Q of the conventional design is ~400. This suggests that the Q in the switched device is not limited by the bridge/AlN interface, but rather by the structure of the switch and feeds. Experiments are underway to determine the cause of the increased loss, but possibilities include increased acoustic damping from the thicker bridge metal and anchor losses from the resonator to the bridges. Also, the most likely cause of the reduced isolation of the MEMS design is edge coupling of the bridges.

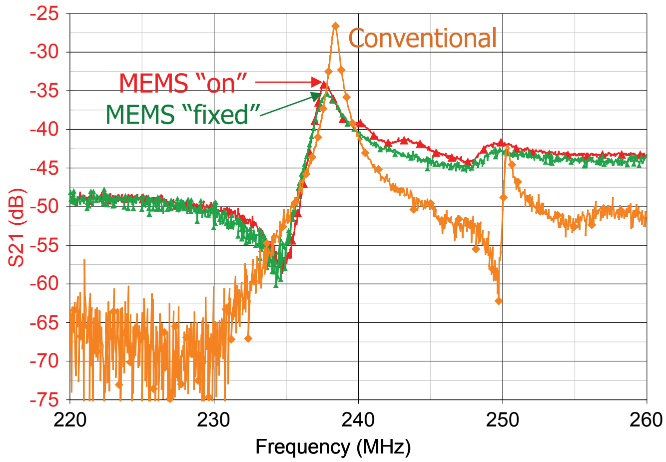

Fig. 6. Insertion loss of the switched MEMS resonator (MEMS “on”) compared to the same structure with fixed-down MEMS switches (MEMS “fixed”) and a conventionally designed resonator with the same finger dimensions (Conventional).

These results demonstrate the ability to change the piezoelectric coupling and transduction of a piezoelectric resonator by varying the gap between a resonator transducer finger and the piezoelectric material. While the device reported here has a relatively simple on-off functionality, it can be extended to reconfigurable high-Q resonators and filters in which frequency, coupling, and bandwidth may be selected by changing which of many fingers are activated in a device. Successfully demonstrating tunable filters with performance equivalent to fixed devices will require improving the MEMS device yield and reliability to allow more switch fingers, reducing the input-output coupling to increase isolation, and improving the device fabrication to increase the Q of the device to that of the intrinsic AlN material.

V. Conclusion

We have demonstrated the first MEMS-switched acoustic resonator as a building block for a new class of adaptive and reconfigurable RF filters. The resonators use a MEMS capacitive switch device to change between an on-state in which the electrodes are closely coupled to the piezoelectric film and an off-state where the electrodes are separated from the film. The switched resonator occupies <0.1 mm^2 of area, shows a Q of 170, a switching ratio of 13 dB, and a center frequency of 238 MHz. The response of the switched resonator is similar to that of a device with fixed-down switches and the same feed structure, suggesting that the performance is not limited by the switch interface, but rather by the feed structure. Ongoing work towards realizing frequency and bandwidth reconfigurable filters includes improving the reliability, yield, Q, isolation, and switching ratio of the MEMS switches and resonator device.

Acknowledgement

Sandia National Laboratories is a multi program laboratory managed and operated by Sandia Corporation, a wholly owned subsidiary of Lockheed Martin Corporation, for the U.S. Department of Energy's National Nuclear Security Administration under contract DE-AC04-94AL85000. This work was supported by the DARPA RF FPGA Program, program manager William Chappell. The authors acknowledge fabrication support by the MESAFab operations team and measurement support by M. Balance and J. Nguyen.

References

[1] R. Vazny, H. Pretl, L. Maurer, and R. Weigel, “Front-End Implications to Multi-Standard Cellular Radios: State-of-the-Art and Future Trends”, *Proc. 2010 IEEE Ultrasonics Symp.,* pp. 95–98, Oct. 2010

[2] E. J. Naglich, J. Lee, D. Peroulis, and W. J. Chappell, “High-tunable bandstop filterswith adaptable bandwidth and pole allocation,” *IEEE MTT-S Int. Microw. Symp. Dig.,* pp. 1–4, Jun. 2011.

[3] C.-C. Cheng and G. M. Rebeiz, “A Three-Pole 1.2-2.6-GHz RF MEMS Tunable Notch Filter With 40-dB Rejection and Bandwidth Control, *IEEE Trans. Microwave Theory & Tech.,* vol. 60, no. 8, pp. 2431-2438, Aug. 2012.

[4] C. T.-C. Nguyen, “MEMS Technology for Timing and Frequency Control,” *IEEE Trans. Ultrasonics, Ferroelectrics, and Freq. Control,* vol. 54, no. 2, pp. 251-270, Feb. 2007.

[5] R. Aigner, “Filter Technologies for converged RF-frontend architectures: SAW, BAW, and beyond,” *Proc. SiRF,* pp. 136-139, Jan. 2010.

[6] C. Zuo, N. Sinha, M. B. Pisani, C. R. Perez, R. Mahameed, and G. Piazza, “Channel-Select RF MEMS Filters Based On Self-Coupled AlN Coupled Contour-Mode Piezoelectric Resonators,” *Proc. 2007 IEEE Intl. Ultrasonics Symp.,* pp. 1156-1159, Oct. 2007.

[7] R. Aigner, “Tunable Acoustic RF-Filters: Discussion of Requirements and Potential Physical Embodiments,” *Proc. European Microwave Conf.,* pp. 787-790, Sept. 2010.

[8] C. L. Goldsmith, D. I. Forehand, Z. Peng, J. C. M. Hwang, and J. L. Ebel, “High-cycle life testing of RF MEMS switches,” *Proc. IEEE MTT-S Int. Microw. Symp.,* pp. 1805–1808, Jun. 2007.

[9] G. M. Rebeiz, *RF MEMS: Theory, Design, and Technology.* New York: Wiley-Interscience, 2003.

[10] M. Fernandez-Bolanos Badia, E. Buitrago, and A. Mihai Ionescu, “RF MEMS Shunt Capacitive Switches Using AlN Compared to Si_3N_4 Dielectric,” *J. Microelectromechanical Systems,* vol. 21, no. 5, pp. 1229-1240, Oct. 2012.

[11] L.-W. Hung and C. T.-C. Nguyen, “Capacitive-Piezoelectric AlN Resonators with Q>12,000,” in *Proc. Intl . Conf, MEMS,* pp. 173-176, Jan. 2011.

[12] W. Pang, H. Zhang, H. Yu, and E. S. Kim, “Electrically Tunable and Switchable Film Bulk Acoustic Resonator,” in *Proc. Freq. Control Symp.,* pp. 22-26, Aug. 2004.

[13] G. Piazza, “Integrated Aluminum Nitride Piezoelectric Microelectromechanical System For Radio Front Ends,” *J. Vac. Sci. Tech. A,* vol. 27, no. 4, pp. 776-784, Jul/Aug 2009.

[14] R. H. Olsson, III, K. E. Wojciechowski, M. S. Baker, M. R. Tuck, and J. G. Fleming, “Post-CMOS-Compatible Aluminum Nitride Resonant MEMS Accelerometers,” *IEEE J. Microelectromech. Sys.,* vol. 18, no. 3, pp, 671-678, June 2009.